Proc. Indian Acad. Sci. (Engg. Sci.), Vol. 6, Pt. 3, September 1983, pp. 233–254.


# Passive microwave remote sensing of the atmosphere and ocean

T A HARIHARAN and P C PANDEY
Space Applications Centre, Ahmedabad 380053, India

**Abstract.** The microwave remote sensing experiments conducted during the last decade using airborne and spaceborne sensors are now evolving as operational spacecraft observation systems. Microwave sounding unit (MSU) onboard TIROS-N regularly provides global atmospheric temperature profile required for numerical weather prediction. The monitoring of composition profile and geophysical parameters from space platform is now a reality and holds a great promise for future meteorological and oceanographic research. This review paper summarises the recent advances and future opportunities in passive microwave radiometry. Indian microwave remote sensing programme and achievements to date are also described.

**Keywords.** Passive microwave radiometry; retrieval technique; atmospheric sounding; terrestrial sounding; satellite microwave radiometer; *Bhaskara* satellite

## 1. Introduction

During the past decade, the achievements from the NEMS (*Nimbus* E microwave spectrometer) and SCAMS (scanning microwave spectrometer) have led to the development of the first operational microwave spectrometer flown on the TIROS-N series of satellites. These satellites carried a four-channel microwave sounding unit (MSU) for sounding the atmosphere. Also, a seven-channel microwave temperature sounder was flown on a Block D meteorological satellite developed by defence meteorological satellite program (DMSP). The launch of SEASAT and *Nimbus*-7 satellites and the successful operation of the various instruments onboard the spacecraft was a great technological advancement. It was a proof of the concept mission and has added a new dimension in our capability of monitoring the ocean from space. Global measurements of sea surface temperature, wind speed, precipitable water and sea-ice coverage with significant accuracies are a reality now and holds a great promise for future operational applications. The principal advantage of microwaves is their relative ability to penetrate clouds, haze, precipitation and surface material such as snow and ice. Besides, other properties unique to microwaves can also be exploited. Tomiyasu (1974), Ulaby (1976), Swift (1980), Staelin (1981) and more recently Njoku (1982) have reviewed the advances in the field of microwave remote sensing of the earth's surface and its atmosphere. The present paper reviews the progress to date in satellite microwave radiometry with emphasis on the current important results obtained from SEASAT SMMR (scanning multichannel microwave radiometer) and SAMIR (satellite microwave radiometer) onboard the second Indian earth observation satellite *Bhaskara*.

## 2. Basic principles of passive microwave radiometry

Thermal radiation emitted by geophysical sources is expressed in terms of brightness temperature $T_B(\nu)$, in units of degrees Kelvin, where $T_B(\nu)$ is the temperature of a black-

body radiator that produces equivalent power at frequency $v$. The values of $T_B(v)$ range between 60 and 305 K for oceans and tropical forests respectively.

The brightness temperature observed from satellite-borne microwave radiometer, is given by radiative transfer theory described in detail by Chandrasekhar (1960)

$$T_B(v) = \left[ T_0\varepsilon + (1-\varepsilon) \int_0^\infty T(h)\alpha(h) \exp\left( - \int_0^{h'} \alpha(h')\,\mathrm{d}h' \right) \mathrm{d}h \right] \exp(-\tau_0)$$

$$+ \int_0^\infty T(h)\alpha(h) \exp\left[ - \int_h^\infty \alpha(h)\,\mathrm{d}h \right] \mathrm{d}h, \tag{1}$$

where $T(h)$ and $\alpha(h)$ are the atmospheric temperature (K) and absorption coefficients ($m^{-1}$) respectively as a function of height $h$. $T_0$ is the surface temperature and $\varepsilon$ is surface emissivity.

$$\tau_0 = \int_0^\infty \alpha(h')\,\mathrm{d}h' = \text{total atmospheric opacity.} \tag{2}$$

In case of scattering from rough surfaces or from atmospheric constituents like hydrometeors, the above equation of radiative transfer is modified (Tsang & Kong 1976). Matrix equation of radiative transfer is required for considering the effect of mesospheric oxygen which is influenced by magnetic field (Lenoir 1967). This will be useful for studying atmospheric constituents using microwave limb sounder.

Equation (1) assumes an approximately specular reflection at the surface. The equation was computed by dividing the atmosphere into concentric layers, each with a specified temperature and absorption coefficient and using a summation to approximate the integrals. Cloud layers can be inserted at any altitude by modifying the absorption coefficients to include an appropriate amount of liquid water. In addition, the relative humidity of the air was assumed to be 100% in the presence of clouds.

The principal absorbing constituents of electromagnetic radiation are $O_2$, $H_2O$, hydrometers, and many trace gases including $O_3$, CO, $H_2O$, $HNO_3$, different oxides of nitrogen, O, OH, ClO, $H_2O_2$ and others. An excellent treatment of the absorption due to various atmospheric gases and trace constituents is described by Waters (1976). The accuracy requirements of various absorption formalisms are adequate for general remote sensing applications but there is still some debate on the role of water vapour dimers and its effect on remote sensing, which may be important if relative humidity is high. This and some other issues like line shape and in some cases line strength require further research.

## 3. Retrieval technique

Geophysical parameter retrieval techniques using multiwavelength microwave radiometric data are statistical (Waters *et al* 1975; Grody 1976; Wilheit & Chang 1980; Hofer & Njoku 1981; Pandey & Kakar 1983), nonlinear iterative (Wentz 1983) and fourier transform technique (Rosenkranz 1978). The most generally used procedure is

statistical, which was first used by Waters (1975) for retrieving atmospheric temperature profile from measurements near 60 GHz $O_2$ band. The principle behind this method is to find the linear predictor $D$

$$\hat{\mathbf{x}} = \vec{\mathbf{D}}\mathbf{y}, \tag{3}$$

by minimising $E\{(\mathbf{x}-\hat{\mathbf{x}})^T(\mathbf{x}-\hat{\mathbf{x}})\}$. $\hat{\mathbf{x}}$ is the estimate of parameter vector and $\mathbf{y}$ is the measurement vector.

This is of course classical problem of multiple linear regression, with elements of $\vec{\mathbf{D}}$ as regression coefficients. The matrix $\vec{\mathbf{D}}$ is given by

$$\vec{\mathbf{D}} = E\{\mathbf{x}\cdot\mathbf{y}^T\}(E\{\mathbf{y}\mathbf{y}^T\})^{-1}. \tag{4}$$

Both the expected values in the above expressions are covariance matrices. Instead of evaluating $\vec{\mathbf{D}}$ as given in (4), sometimes it is more convenient to subtract mean of $x$ and $y$ to obtain the covariance matrices. If we have a large sample of measured $\mathbf{Y}$ with our radiometer and also have independent direct measurements from radiosonde, ships or rocketsonde, then we can estimate $\vec{\mathbf{D}}$ entirely from experiment. Otherwise radiative transfer modelling with known physics and the *a priori* statistics is used to estimate $\vec{\mathbf{D}}$.

Incorporation of a few nonlinear terms in the above retrieval can, sometime, improve the accuracy (Sharma *et al* 1981; Rosenkranz *et al* 1972). In the temperature profile retrieval, an improvement of $10 \sim 30\%$ is obtained using Kalman filtering technique (Ledsham & Staelin 1978). However this technique has not been applied to retrieve geophysical parameters from multiwavelength measurements and holds promise for future research in this area. For nonlinear problems, analytical technique developed by Chahine (1977) can also be used, specially for profiling of water vapour, temperature and atmospheric composition.

## 4. Geophysical applications

### 4.1 *Atmospheric sounding*

Waters *et al* (1975) reported the first retrieval of temperature profile from NEMS onboard *Nimbus*-5 satellite. This instrument measured atmospheric radiation near 60 GHz oxygen band. The mixing ratio of oxygen in the atmosphere is quite uniform and time-invariant; thus measurement of atmospheric emission at $\sim$ 60 GHz is proportional to atmospheric temperature at altitude levels defined by temperature weighting functions (Meeks & Lilley 1963). The three frequencies used for temperature retrievals were 53·65, 54·9 and 58·8 GHz. In addition, two more channels 22·235 and 31·4 GHz were also used for precipitable water retrieval.

The NEMS instruments for temperature retrieval were further improved and were followed by similar instruments with more number of channels on TIROS series and the block 5D satellites. A typical weighting function for block 5D temperature sounder is shown in figure 1.

The NEMS results have demonstrated the potential of passive microwave techniques for remote sensing of atmospheric temperatures from earth orbiting satellites. An RMS accuracy of $\sim$ 2°K has been reported by Waters (1975) based on comparison of NEMS-

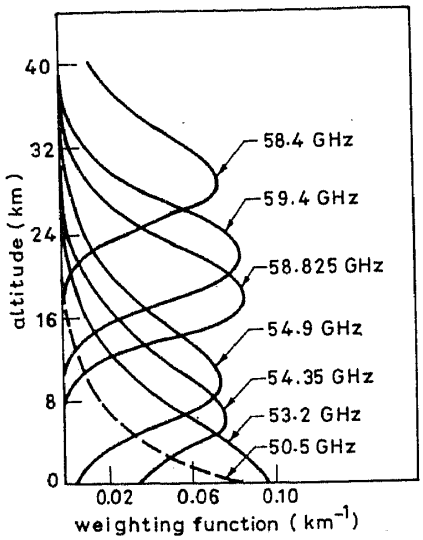


**Figure 1.** Atmospheric weighting function for a downward looking radiometer with an assumed calm sea background for SSM/T on-board block 5D satellite.

derived temperature profile with ground truth data obtained from the National Meteorological Centre (NMC) operational analysis and radiosondes. Figure 2 shows NEMS temperature retrieval and RMS variation.

The effect of clouds on temperature retrieval was also investigated by Staelin *et al* (1975) and it was found that clouds affect less than 0·5% of the sounding; the sounding affected most is centred around inter-tropical convergence zone (ITCZ). They also observed a high correlation between 53·65 GHz brightness temperature and NEMS inferred liquid water. Figure 3 shows the result.

Further, improvements in temperature profile retrieval are expected with approximately 13 channels advanced instruments, currently under study in USA and proposed for possible deployment in late 1980. Several important research areas need further attention in order to improve the retrieval. Development of retrieval technique using hybrid data *i.e.* data from MW and IR sensors, effect of clouds and rain on the

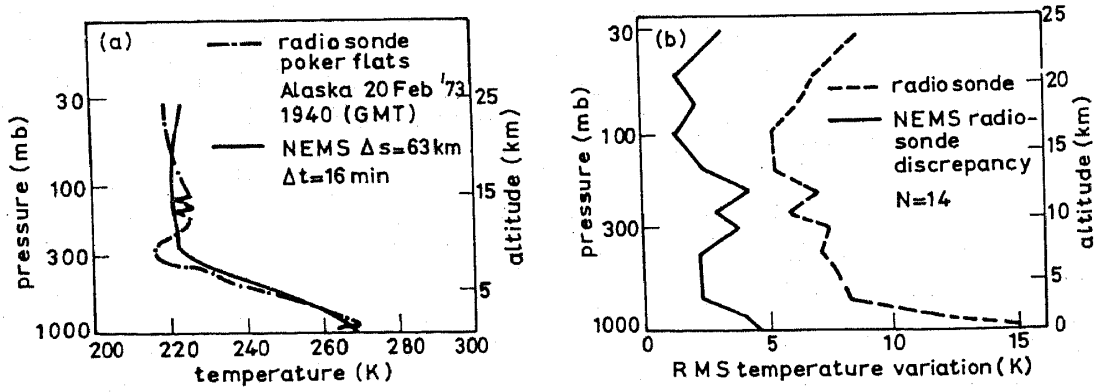


**Figure 2.** (a) Comparison of NEMS retrieved temperature profile with coincident radiosonde (b) RMS temperature variation in radiosonde measurements and RMS discrepancies between radiosonde and NEMS for Ft. Churchil Soundings (after Waters *et al* 1975).

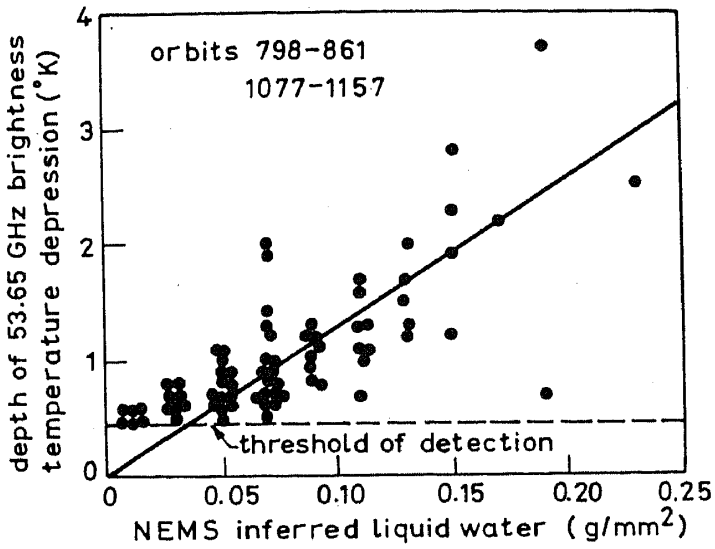


**Figure 3.** Correlation between the depth of the 53·65 GHz brightness temperature depression and NEMS inferred liquid water abundance for depressions above threshold of detection, over ocean (after Staelin *et al* 1975).

retrieval, understanding the difference between simulated radiance with known profiles and the measured radiances, correction for surface effects like snow-capped mountains etc, require immediate attention.

Staelin *et al* (1976) and Grody (1976) used the water vapour channels for determining integrated atmospheric water vapour and liquid water abundances using regression approach. The retrieval accuracy for precipitable water was established by comparing NEMS derived water vapour with radiosonde's launched from ships and small islands. An RMS accuracy of $\sim 0{\cdot}4$ g/cm$^2$ was obtained for water vapour and theoretical RMS accuracy of $\sim 0{\cdot}01$ g/cm$^2$ was obtained for liquid water since there was no experimental comparison for liquid water.

The NEMS water vapour channels were also used for snow and ice studies by Kunzi *et al* (1976). Possibility of distinguishing different types of snow and ice was demonstrated.

Figure 4(b) shows the liquid water content and water vapour content through tropical depression over Pacific ocean as determined from NEMS measurements. Within the tropical environment, knowledge of the large variations of water vapour is of utmost importance for understanding of tropical cyclones and cloud clusters (Ruprecht & Gray 1976). However, most numerical prediction models require at least two vertical layers of water vapour amounts in the atmosphere rather than total values of water vapour. Development of the radiometers employing $\sim$ 183 GHz strong water vapour line and more transparent 22 GHz line would provide moisture profile required for numerical weather prediction. Research effort in this direction is in progress both in terms of instrument development as well as profile retrieval technique (Schaerer & Wilheit 1979; Rosenkranz & Staelin 1982). Although no spacecraft aircraft experiment has demonstrated this technique, theoretical simulation shows an accuracy of $\sim 20\%$ per 2–3 km layer assuming known temperature profile to an accuracy of the $\sim 1{\cdot}5$ K. Careful study and actual experiment is required for a more definitive results. Haydu & Krishnamurty (1981) have demonstrated the use of radiosonde data and

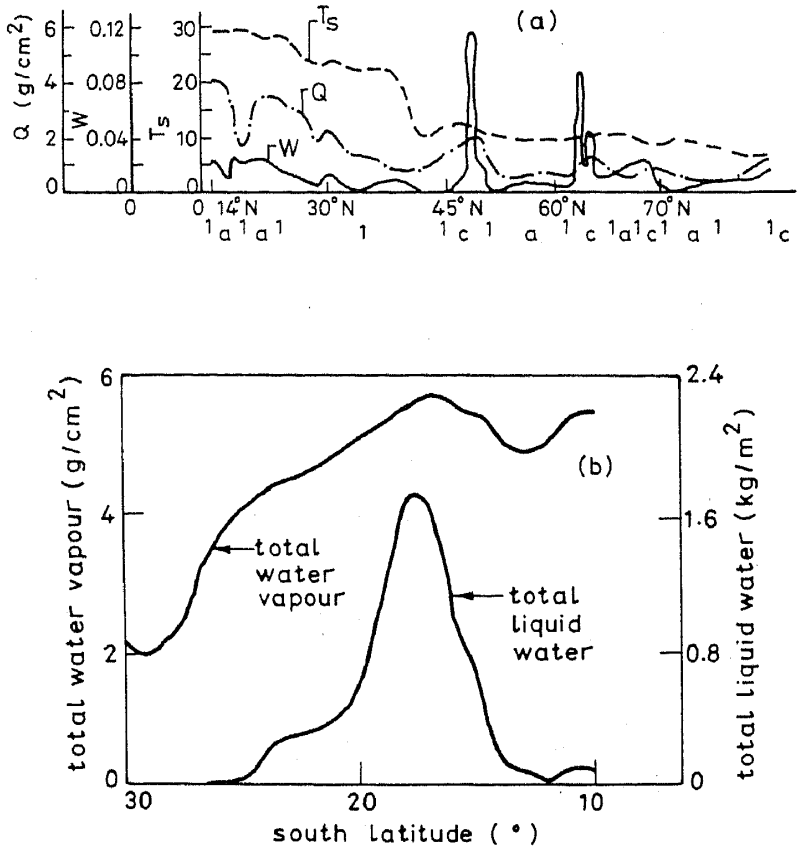


**Figure 4.** **a** Profiles of the ocean-surface temperature $T_s$, the moisture content pattern of the air $Q$ and the hydrometer field obtained over the Atlantic. W—total water content c—continuous cloud cover; a—appreciable cloud cover, l—slight cloud cover. **b** Liquid water content and water vapour content through tropical depression over Pacific ocean as determined from NEMS measurements (Grody 1976).

spectrometer data for water vapour profile retrieval making certain simplifying assumptions. SEASAT scanning multichannel microwave radiometer (SMMR) which was launched in 1978 measured microwave radiation at 6·6, 10·69, 18, 21 and 37 GHz and in both horizontal and vertical polarisations. The results of the SEASAT-SMMR are reported in various workshop reports published by the Jet Propulsion Laboratory, USA (for example, see Lipes 1980). Precipitable water vapour from SMMR was obtained on much finer resolution and global maps were produced. Figure 5 is an example of global

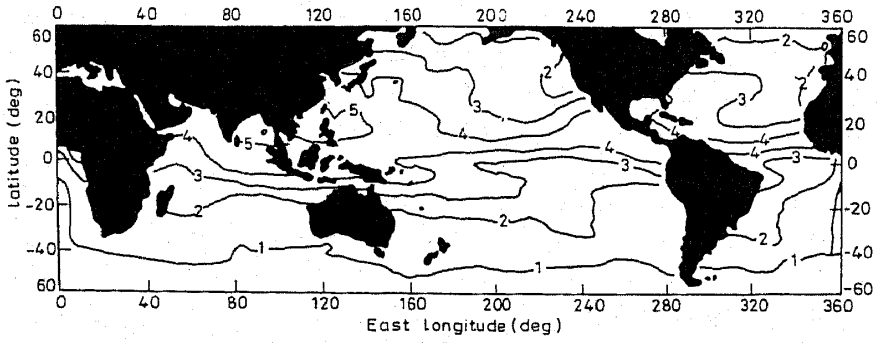


**Figure 5.** Global SEASAT-SMMR mean monthly moisture field for the period 7 July–6 August 1978 (after Pandey 1982).

distribution of water vapour obtained from SEASAT-SMMR data. Major large scale features are noticeable which are possibly connected with large scale general circulation (Prabhakara *et al* 1982; Alishouse 1982).

A very active research programme in measuring stratospheric constituents $O_3$, ClO and $H_2O_2$, among others, is being pursued at the Jet Propulsion Laboratory by Waters and his colleagues using limb-sounding technique. Already balloon-borne radiometers have given important results (Waters *et al* 1976, Waters & Wofsky 1978). Also spaceborne limb sounding radiometers operating at microwave and millimeter wavelengths are under development and planned for upper atmospheric research satellite proposed for the late 1980's. The data from these sounders will enhance our capability to understand the chemistry of the upper atmosphere. Monitoring of temporal and spatial distribution of $O_3$ will address the global habitability problem and the possible effect of harmful UV on human skin causing cancer.

Geostrophic winds from three-dimensional temperature fields have been proposed by Grody *et al* (1979) and demonstrated by SCAMS observations. Waters & Wofsy (1978) proposed measurement of Doppler shifts *via* limb scanning for geostrophic wind estimation.

### 4.2 *Terrestrial sensing*

The application of the passive microwave radiometry for earth resources applications and land applications is not as promising as oceanic applications so far. Although soil moisture, snow and sea ice have been studied using passive technique, oceanographic parameters received the highest priority using passive microwave technique. The success of SEASAT oceanographic mission, with three active sensors, altimeter, scatterometer, synthetic aperture radar, a scanning multichannel microwave radiometer and an infrared sensor to identify major cloud feature for data interpretation from other active and passive sensors, has created an international interest. The future generation of ocean-monitoring satellites will undoubtedly deploy passive microwave sensors because of the demonstrated capability of SEASAT SMMR.

The SEASAT-SMMR provided sea surface temperature, wind speed, precipitable water, rain rate and sea-ice concentration. The SMMR instruments are described in detail by Gloersen & Barath (1977) and Njoku *et al* (1980b). Swanson & Riley (1980) describe the calibration of SMMR instruments based on physical modelling of the various losses in the waveguide and thermovac data. Before the geophysical processing, antenna temperatures are used as input for antenna pattern correction algorithm, developed by Njoku *et al* (1980a). The antenna pattern algorithm reformats the data, compensates for antenna sidelobes and cross-polarisation effects and finally brightness temperature data are used for geophysical processing. Lipes *et al* (1979) and Hofer *et al* (1981) have described the results of comparison of SEASAT-SMMR derived geophysical parameters and the data from other sources. Point comparison of sea surface temperature (SST) obtained from SEASAT-SMMR and *in situ* measurements showed an RMS difference of $\sim$ 1·2 to 1·5°K based on different database for comparisons (Hofer *et al* 1981 and Pandey & Kakar 1983). Different subsets of brightness temperatures are used for retrieval of a given geophysical parameter. Global maps of SST are produced and compared with climatological maps. An example of mean monthly map of SST and the corresponding SST climatological map as obtained by Pandey & Njoku (1982) using SEASAT-SMMR data

is given in figure 6. An attempt is made here to ensure the reliable reproduction of SST anomalies which could be used for weather forecasting and climatic studies. These contours compare favourably with climatological contours. However, the contours near coastal regions and inland waters may be considered with suspicion but in areas ~ 600 km away from main island, the contours are believed to be reliable to within about 1–1·5 K. Further advances have also been made to evaluate the effectiveness of one to three-channel subset in retrieving SST (Pandey & Kniffen 1982). More comparisons and evaluation under different weather conditions are required before one can conclude the ultimate capability of these subsets. This, if found satisfactory, will reduce the cost of instrumentation in future generation of satellites.

SST, being an important element of oceanic processes and studies relating to weather and climate, NASA is currently emphasising on its global measurements from space. A series of workshops, chaired by Dr E G Njoku of Jet Propulsion Laboratory has been planned to evaluate different sensors in infrared and microwave region for SST measurement. The outcome of this workshop will be valuable for future research in SST and also the new sensors to be flown on future spacecraft for SST estimation. This should be considered a very auspicious development.

Global measurements of wind speed using SEASAT-SMMR data are given in figure 7 for the period 7 July to 6 August 1978. Point comparison with *in situ* observations showed an RMS accuracy of ~ 1·5 m/s using a two-channel subset of 10 H, 10 V channels.

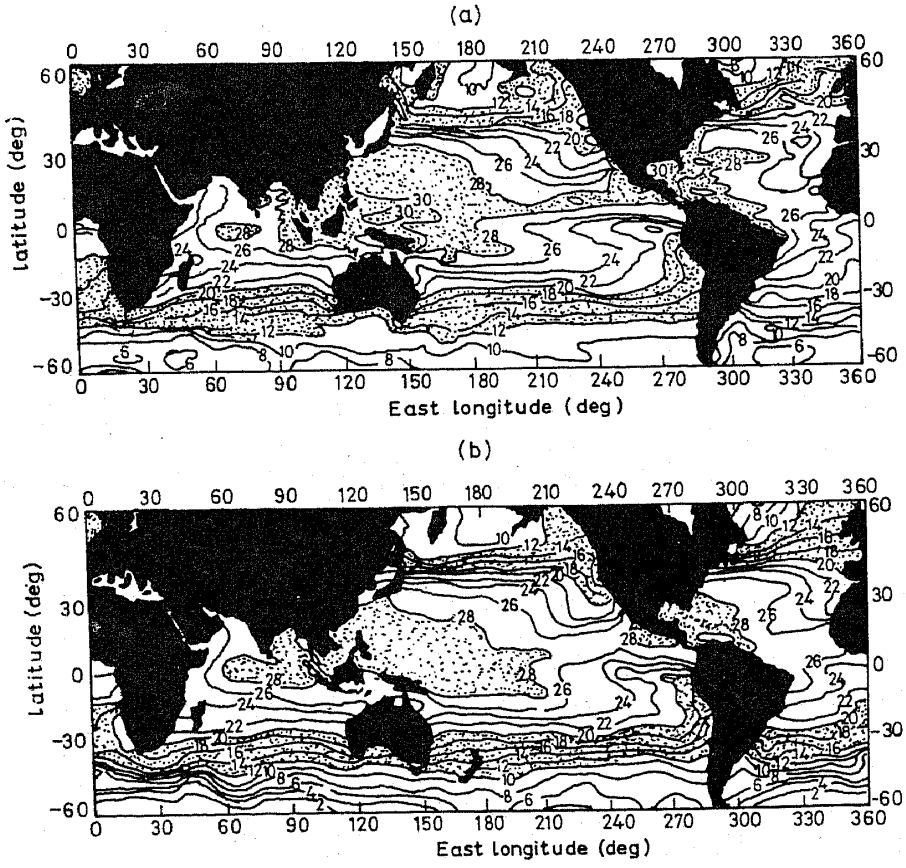


**Figure 6.** (a) SEASAT-SMMR SST for the month of August 1978 (Pandey & Njoku 1982). (b) Climatological SST map for the month of August 1982 (Pandey & Njoku 1982).

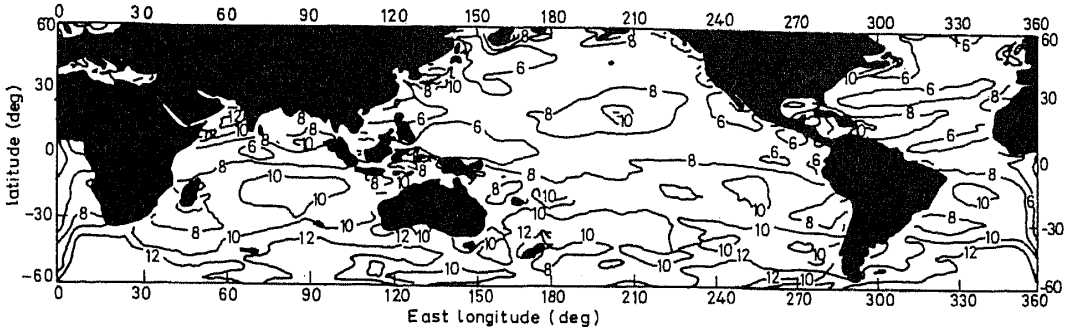


**Figure 7.** SEASAT-SMMR wind speed for the period 7 July–6 August 1978 (Pandey 1983).

However, comparison in different regions of the ocean for SEASAT mission showed an overall accuracy of ~ 2·5 m/s using Chester's algorithm, currently being used at the Jet Propulsion Laboratory, which is the ultimate retrieval accuracy envisaged from SEASAT-SMMR. Comparisons of SMMR wind speed with SEASAT-altimeter and scatterometer wind speed have shown good general agreement but some biases were observed in high latitude winds (Pandey 1983). These discrepancies might be due to different spatial resolution of the sensors which provide different averages if the winds are inhomogeneous within the field of view. Another reason for discrepancies may be the different physical processes responsible for providing their signatures for active (altimeter and scatterometer) and passive (SMMR) sensors (Bernstein 1982). More theoretical and experimental work is required. Continuous analysis of data from *Nimbus*-7 will enable us to assess the usefulness of these parameters for oceanographic and weather and climate research.

The effect of various atmospheric constituents on brightness temperature is well understood. The temperature and salinity affects brightness temperature *via* complex dielectric constant of seawater. However, the effect of wind which generates wave spectrum and foam, on brightness temperature are not well understood. Although several theoretical models have been proposed to explain the Tb *vs* wind speed dependence (Wentz *et al* 1981), the empirical results have been more widely accepted (Hollinger 1971; Swift 1974; Wilheit 1979; Pandey & Kakar 1983).

Moore *et al* (1975) reported the studies of soil moisture with microwave radiometer onboard *Skylab*. Ulaby *et al* (1975) further compared data from the S-193, S-194 (1·4 GHz) and electrically scanning microwave radiometer (ESMR), 19·35 GHz, sensors over the Utah Great Salt Lake Desert. Within this region large decrease in brightness temperature and increase in scattering coefficients were observed as a result of the smooth, bare nature of the surface. Results from scatterometer portion of the instrument are discussed in more detail by Moore & Young (1977). Soil moisture determination is possible because of reduction of soil microwave emissivity. Schmugge *et al* (1974) have suggested frequencies near ~ 1·4 GHz for soil moisture determination. The effect of roughness and vegetation provide additional complication on soil moisture estimation and both active and passive microwave techniques are currently under study for this purpose (Schmugge 1978) and more research effort is required to determine the ultimate accuracy and operational potential.

Oil slick thickness and its volume can now be measured directly using multi-frequency microwave radiometers (Hollinger & Mannella 1973). Laboratory measurements have indicated an accuracy of ~ 20% in thickness measurements for oil

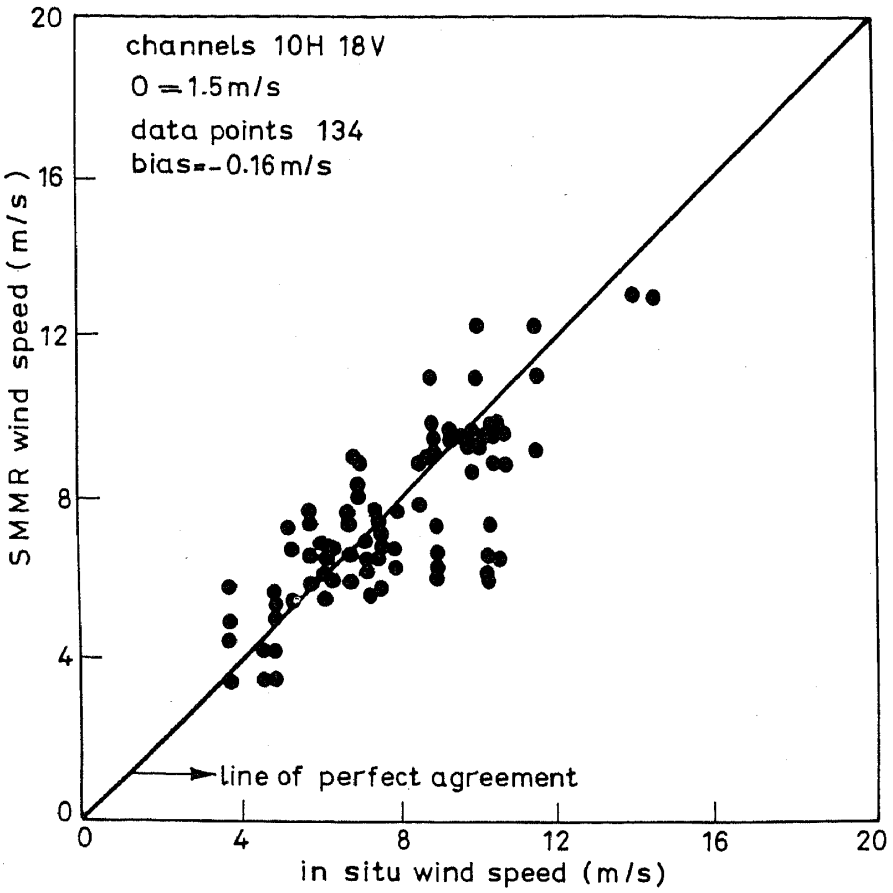


**Figure 8.** SMMR wind speed comparisons with JASIN surface measurements (Pandey 1983).

thickness of 7 to 25 mm and a single frequency radiometer operating in the frequency range of 2–8 GHz has been recommended (Hollinger & Kenney 1976). Figure 9 shows the oil thickness derived from average antenna temperature at both 22·2 and 31·4 GHz versus the expected average thickness.

Microwave pressure sounder (MPS) program is being pursued at the Jet Propulsion Laboratory to determine surface pressure with an accuracy of few millibars (Flower &

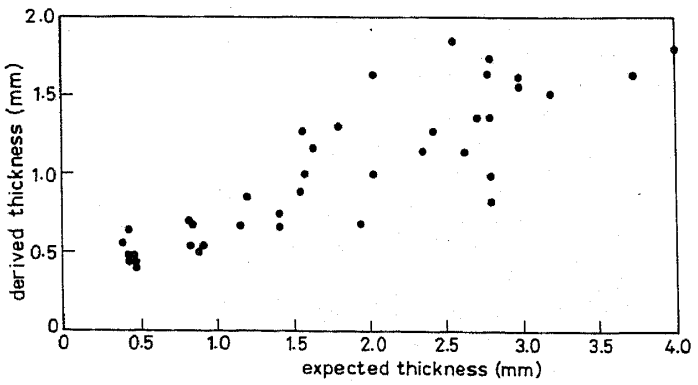


**Figure 9.** Oil film thickness derived from the average antenna temperature at both 22·2 and 31·4 GHz versus the expected average thickness (Hollinger & Kenney 1976).

Pekham 1983). The technique utilises the differential absorption of radar signals at nadir over oceans at two closely-spaced frequencies in the pressure broadened wing of 50–70 GHz $O_2$ absorption band. Aircraft flights were conducted by JPL scientists (Flower & Pekham 1983) and initial results show great promise.

Rainfall rate is another important and difficult parameter to be measured from space. A model for quantitatively relating microwave brightness temperature to rain rate over oceanic area was developed by Wilheit *et al* (1977). In their model at 19·35 GHz, the rain is treated as a Marshal–Palmer distribution of rain drops extending from surface to freezing level, with appropriate water vapour and non-raining cloud distributions. The full mie scattering and absorption properties of the ensemble of droplets are calculated and the equation of radiative transfer is solved with iteration to account for scattering. The quoted accuracy of this model is $\sim 100\,\%$. Rainfall in tropical cyclone has also been reported (Allison *et al* 1974). Another interesting and useful development is $\sim 90$ GHz measurement from defence meteorological satellite program ($\sim$ 1984–86) to estimate rainfall rate over both oceans and land. The initial studies have been reported by Savage (1976). A workshop conducted at GSFC point out a number of recommendations using both active and passive microwave sensors and using both infrared and microwave sensors (Atlas & Thiele 1982). A hybrid technique might be useful but more theoretical and experimental work is recommended (Savage 1976; Weinman & Davies 1978) and is in progress to understand this complex phenomenon from space platform.

## 5. Radiometer system concepts

Although microwave radiometers in general have different characteristics depending upon the type of applications, there are basically two types of receivers: (i) the total power radiometer and (ii) the Dicke comparison radiometer. All these radiometers have basically three subsystems in common (a) an antenna and scan subsystem which receive radiation from the source (b) a radiometer receiver and electronics subsystem which amplifies and detects the signal (c) a data and control subsystem for transmission of radiometric and other relevant housekeeping data etc. A recent text book by Ulaby (1981) describe in detail the radiometer fundamentals.

### 5.1 *Total power radiometer*

Figure 10(a) shows the block diagram of the total power radiometer system. The RMS uncertainty in detecting the signal is given by

$$\Delta T_{\min} = (T_s + T_{rn})\left[\frac{1}{B\tau} + \left(\frac{\Delta G}{G}\right)^2\right]^{1/2}.$$

The symbols are described in figure 10a. $\Delta G$ is the RMS value of the detected receiver power-gain variations. $T_{rn}$ is the internally generated receiver noise. This total power radiometer results in sensitivity improvements by a factor of 2 and is simple in concept and does not have Dicke switch and demodulator. The disadvantage is that variations in output level caused by gain variations and bandwidth variations are not compensated for. Recent advances, however, in component technology and circuit design has

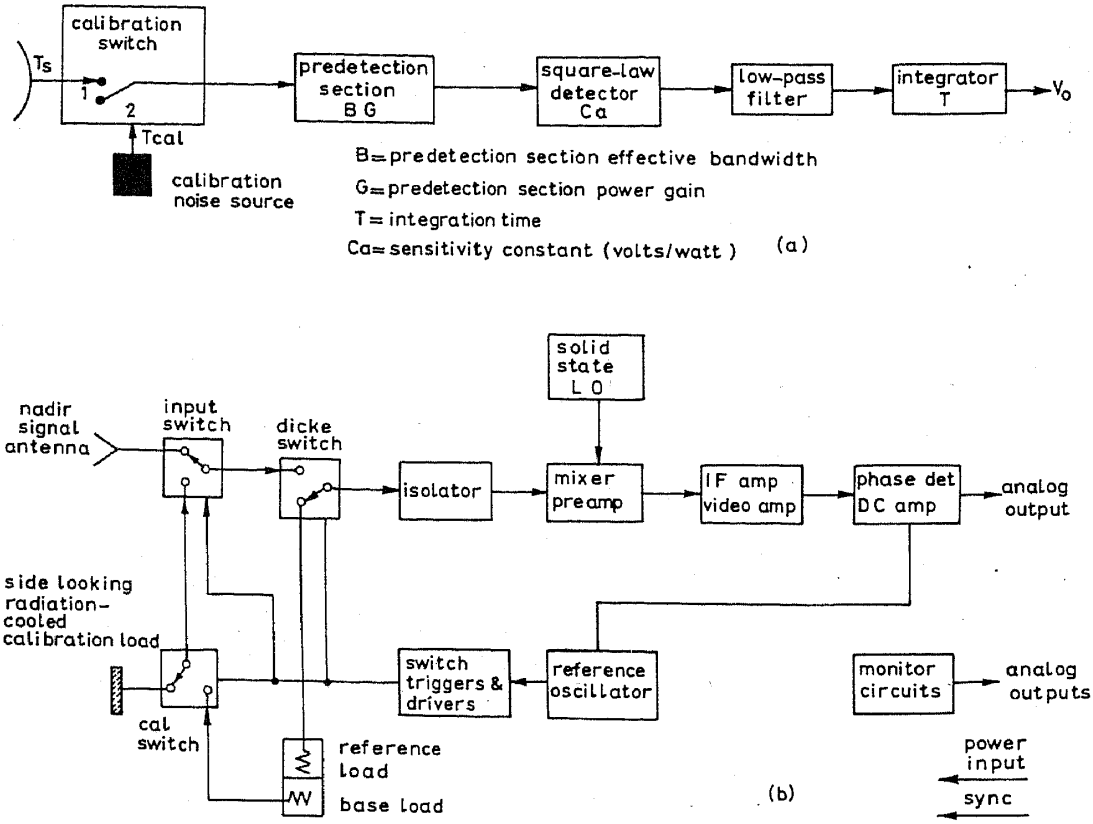


**Figure 10.** (**a**) Total power radiometer (Ulaby 1976). (**b**) Dicke comparison radiometer (as implemented on *Nimbus*-5 (Njoku 1982).

improved stability to the point where total power radiometers are now being implemented in design for future satellite radiometer systems (Hughes Aircraft Co 1979).

### 5.2 *Dicke comparison radiometer*

Figure 10(b) shows the block diagram of the Dicke comparison radiometer which has been used most for various satellite-based applications. The receiver input is periodically switched between the antenna ($T_s$) and a comparison noise source ($T_c$) at a switching frequency $f_s$. By choosing $f_s$ ($\sim$ 1 kHz) higher than the highest significant spectral component of gain variation spectrum, the effect of gain variations is reduced significantly. The critical receiver parameters in determining the temperature sensitivity $\Delta T_{\min}$ is given by

$$\Delta T_{\min} = \frac{2(T_A + T_{rn})}{(B\tau)^{1/2}},$$

where $T_A$ is the antenna temperature, $B$ is the predetection bandwidth and $\tau$ is the integration time and a square wave modulation has been used.

An advanced concept of scanning mechanism in future generation of satellites has been proposed by the JPL scientists and is described by Njoku (1982) which, it is hoped,

will greatly simplify data processing algorithm and improve the accuracy of retrieval of geophysical parameters from brightness temperature measurements.

## 6. Indian passive microwave radiometry program

### 6.1 *Historical perspective*

Table 1 shows the history of microwave radiometry on spacecraft taken from Staelin (1981). India's involvement in passive microwave radiometry began in June 1979, with the launch of its first experimental earth observation satellite called *Bhaskara-I* which was later followed by another similar satellite called *Bhaskara-II*, launched on 20 November, 1981. Thus, in comparison with the first launch of *Cosmos*-243, in 1968 which carried onboard four-frequency radiometer (3·5, 8·8, 22·2 and 37·5 GHz) for terrestrial remote sensing applications, India's experience is quite recent. Both *Bhaskara-I* and *II* were launched in near circular orbits at an average altitude of $\sim$ 550 km and an inclination of $\sim$ 51°. Both *Bhaskara* satellites are spin-stabilised with onboard control system for spin-rate and spin-axis orientation. The two primary payloads onboard *Bhaskara* satellites were TV camera and satellite microwave radiometer called SAMIR. Their primary objectives were to monitor earth resources and measure total precipitable water vapour and liquid water content over the vast oceanic region surrounding Indian subcontinent in relation to the Indian monsoon.

The SAMIR on board *Bhaskara* satellites were of Dicke-type superheterodyne receivers most commonly used in earlier satellites for different applications. Table 2 summarises the technical specifications of both radiometers SAMIR-I and SAMIR-II. SAMIR-II has 3-channel radiometers 19·35, 22·235 and 31·4 GHz; otherwise their configuration is similar to SAMIR-I. Channel 3 (31·4 GHz) was added to have a better water vapour and liquid water separability (Pandey *et al* 1980).

Both *Bhaskara-I* and *II* were designed to operate the SAMIR system in normal and alternate modes. In the normal mode of operation, the spin axis was maintained perpendicular to the orbital plane, collecting the earth radiation data along the subsatellite track at different incidence angles. Only vertical polarisation radiation were picked up by the radiometers. In case of alternate mode, the spin-axis of the satellite was oriented tangentially to the orbital plane at certain latitude and hence cross-track scanning was achieved. The data analysis of alternate mode was complicated by the polarisation mixing at antenna port which would be larger at higher incidence angles. The deviation of the spin axis from the line tangential to the orbital plane would further contribute to the polarisation mixing. Compensation for polarisation mixing and side lobe correction are two important steps in data processing before reliable geophysical parameter is retrieved. Figures 11(a) and (b) shows the SAMIR coverage from *Baskara-II* satellites in both modes.

The antenna temperature and hence, brightness temperature, was obtained from raw radiometric data using prelaunch calibration algorithm using thermovac data. However, no detailed physical modelling of the radiative losses of the various waveguide components was incorporated into the calibration equation. This simple approach of calibration was preferred over the most sophisticated calibration approach used on earlier satellites, although effort is continuing to understand and implement

**Table 1.** History of microwave radiometry on spacecraft (after Staelin 1981; Njoku 1982; with additions)

| Year of launch | Spacecraft/instrument acronym | Frequencies (GHz) | Antenna type | Smallest-resolution element (km) | Principal parameters measured or inferred |
|---|---|---|---|---|---|
| 1962 | *Mariner* 2 (*Venus flyby*) | 15·8, 22·2 | Mechanically-scanned parabola | 13000 | Limb darkening of planetary emission |
| 1968 | *Cosmos* 243 | 3·5, 8·8 22·2, 37 | Nadir-viewing horns | 13 | Atmosphere: water-vapour content, liquid-water content |
| 1970 | *Cosmos* 384 | — | — | — | Surface: sea temperature, sea-ice concentration |
| 1972 | *Nimbus* 5 ESMR | 19·3 | Electrically-scanned array | 25 | Atmosphere: rain rate surface: sea-ice concentration, ice classification, snow cover |
| | NEMS | 22·2, 31·4 53·6, 54·9 58·8 | Five lens loaded horns, nadir-viewing | 200 | Atmosphere: temperature profile, water-vapour content, liquid water content. Surface: ice classification, snow cover |
| 1973 | *Skylab* S193 | 13·9 | Mechanically scanned parabola | 16 | Surface: soil moisture, ocean winds atmosphere: rain rate |
| | S194 | 1·4 | Nadir-viewing phased array | 115 | Surface: soil moisture |
| 1974 | *Meteor* | 37 | Dual polarisation 30° from nadir | — | Atmosphere: liquid water content |
| 1975 | *Nimbus* 6 ESMR | 37 | Dual polarisation electrically scanned array | 20 × 43 | Same as *Nimbus* 5 ESMR |
| | SCAMS | 22·2, 31·6, 52·8, 53·8, 55·4 | Three rotating hyperbolic mirrors | 150 | Same as *Nimbus* 5 NEMS |

| | | | | | |
|---|---|---|---|---|---|
| 1978 | DMSP SSM/T | 50·5, 53·2, 54·3, 54·9, 58·4, 58·8, 59·4 | Single rotating mirror | 175 | Atmosphere: temperature profile |
| 1978 | TIROS-N/MSU (2 satellites) | 50·3, 53·7, 55·0, 57·9 | Dual rotating mirrors | 110 | Atmosphere: temperature profile |
| 1978 | *Nimbus*-7 SMMR | 6·6, 10·7, 18, 21, 37 | Single oscillating offset parabolic reflector | 18 × 27 | Atmosphere: water vapour content, liquid water content, rain rate |
| | SEASAT 1 SMMR | — | — | 14 × 21 | Surface: sea state (wind speed), sea temperature, sea-ice concentration, ice classification, snow cover, soil moisture |
| 1979 | *Bhaskara-I* SAMIR | 19·4, 22·2 | Lens corrected horns | 150<br>230 | Atmosphere: water vapour content, liquid water content |
| 1981 | *Bhaskara-II* SAMIR | 19·4, 22·2, 31·4 | Lens corrected horns | 150 | Atmosphere: water vapour content, liquid water content<br>Surface: ocean winds |
| 1983 (planned) | DMSP SSM/1 | 19·1, 22·3, 37·0, 85·5 | Continuously rotating offset parabolic reflector | 16 × 14 | Precipitation rate over ocean/land, ocean wind speed, ice type/concentrations, soil moisture. |
| 1986 (planned) | TIROS-O AMSU | 18·5, 22·2, 31·6, 50·3–57·9 (7 ch), 90, 150, 183·3 (3 ch) | Continuously scanned mirrors | 15 | Atmospheric temperature and water vapour profiles |

**Table 2.** Characteristics of the SAMIR systems onboard *Bhaskara-I* and *II*.

| System parameter | B | *Bhaskara-I* radiometers | | *Bhaskara-II* radiometer | | |
|---|---|---|---|---|---|---|
| | R-1 | R-2 | R-3 | R-1 | R-2 | R-3 |
| Frequency (GHz) | 19·1 | 19·6 | 22·235 | 31·4 | 19·35 | 22·235 |
| RF bandwidth (MHz) | 250 | 250 | 250 | 250 | 250 | 250 |
| Integration time (ms) | 350 | 350 | 470 | 300 | 300 | 300 |
| RMS temperature sensitivity T(°K) | 1 | 1 | 1 | 1 | 1 | 1 |
| System noise figure (dB) | 6·5 | 6·5 | 7·5 | 8·5 | 6·5 | 7·5 |
| Spatial resolution (KM) | 150 | 150 | 230 | 125 | 125 | 125 |
| Vie angles with 180° (zenith) respect to nadir (normal mode) | ±2·8°, ±5·6° | | ±2·8°, ±11·2° | ±2·8°, ±5·6°, | | |
| | 180° (zenith) | | 180° (zenith) | 180° (zenith) | | |
| View angles with respect to nadir (alternate mode) | ±2·8°, ±8·4°, ±14·0°, ±19·6°, ±25·2°, ±30·8°, ±36·4° | | | | | |

more advanced calibration algorithms in our future generation of satellites. The sensitivity of the radiometers was estimated to be ~ 1·5 K and found to be stable for long period of operations.

### 6.2 *Some examples of results from* SAMIR *onboard Bhaskara:*

The brightness temperature data obtained from SAMIR-I onboard *Bhaskara-I* satellite gave the first major opportunity to Indian scientists to work with real radiometric data and develop retrieval techniques to obtain geophysical parameters. Radiative transfer formalism was developed and attempts were made to understand the sensitivity of different geophysical parameters on brightness temperature (Pandey *et al* 1980b). This has given us the confidence to optimise the channels for future missions.

The SAMIR sensors (both I and II) measured microwave radiation near water vapour resonance line at 22·235. These channels are primarily affected by water vapour and liquid water (19·35 GHz is affected by rain rate) and in a secondary way by surface winds. As such water vapour and liquid water are two important parameters determined from SAMIR data. These two parameters were obtained by operating on the observed brightness temperature spectra (vectors) with a linear matrix deduced from physics and the *a priori* atmospheric statistics (Pandey *et al* 1981). The technique and its variations have been used earlier by Waters *et al* (1975), Grody (1976), Wilheit & Chang (1980), Hofer & Njoku (1981) and Pandey & Kakar (1983) for similar retrieval problems.

In addition, an empirical approach (Pandey *et al* 1980a) and a variant of regular regression approach, called simulation method were also developed (Pandey *et al* 1981) and used in deriving integrated water vapour and liquid water contents. The three

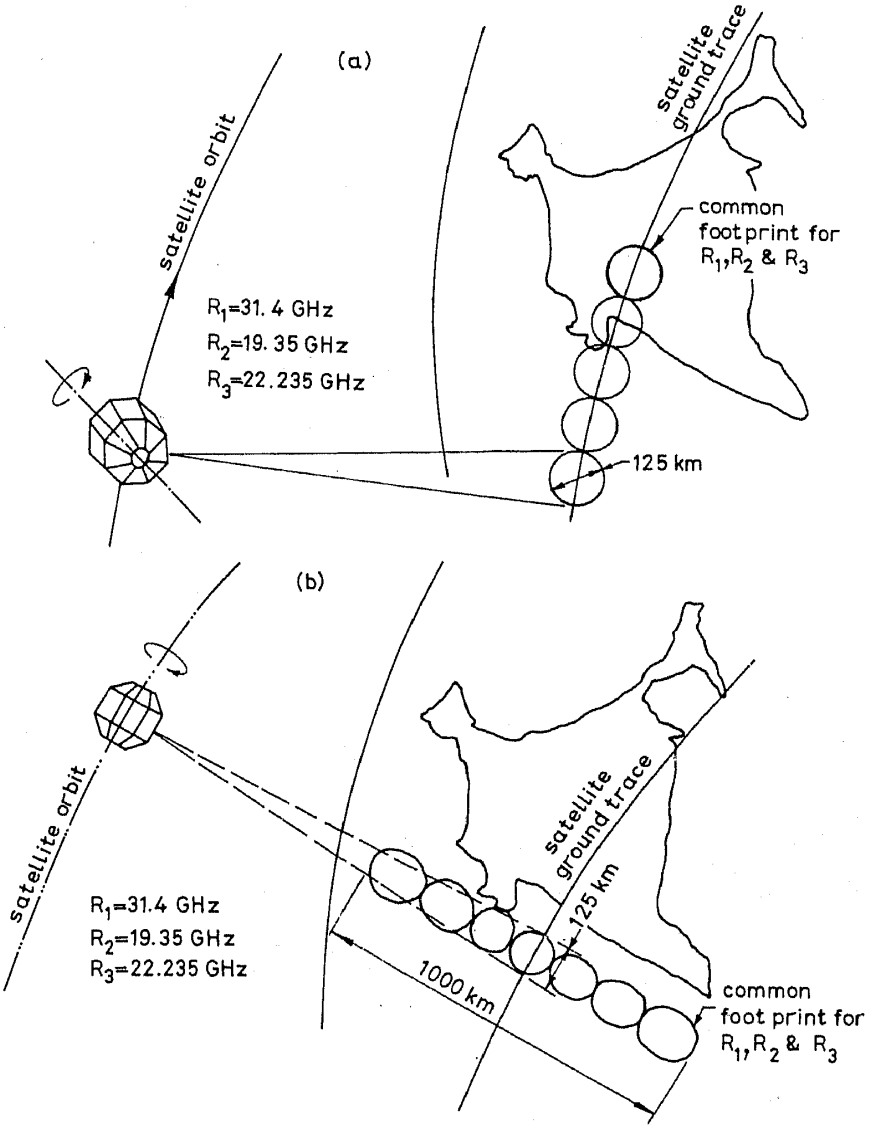


**Figure 11.** *Bhaskara-II* SAMIR coverage in (**a**) normal mode (**b**) alternate mode.

techniques and the intercomparison of the results of deriving water vapour (WV) and liquid water (LW) are described by Gohil *et al* (1981a) and some examples of comparisons are given in figures 12(a), (b) and(c). These analyses indicated an RMS error of $\sim 0{\cdot}4$ g/cm$^2$ in WV estimation after removing the biases. The biases resulted from instrument calibration and inadequate modelling of wind speed *vs* emissivity relationship. The ground truth obtained for comparison was available from MONEX-79 data. In the absence of *in situ* cloud liquid water content measurements, the theoretical RMS accuracy of liquid water determination was estimated to be $\sim 0{\cdot}01$ g/cm$^2$. The range of cloud liquid water values retrieved by SAMIR was in the range predicted by some of the earlier sensors on *Nimbus* (Wilheit *et al* 1980, Staelin *et al* 1976, Grody 1976) satellites.

The onset of Indian monsoon was studied by observing the movement of WV contours, obtained from SAMIR as well as TIROS-N data (Narayanan & Rao 1982) and is described by Desai (1982) along with some other similar studies concerning moisture fluxes and its relation to rainfall and onset dates of the monsoon. Variations of WV in a

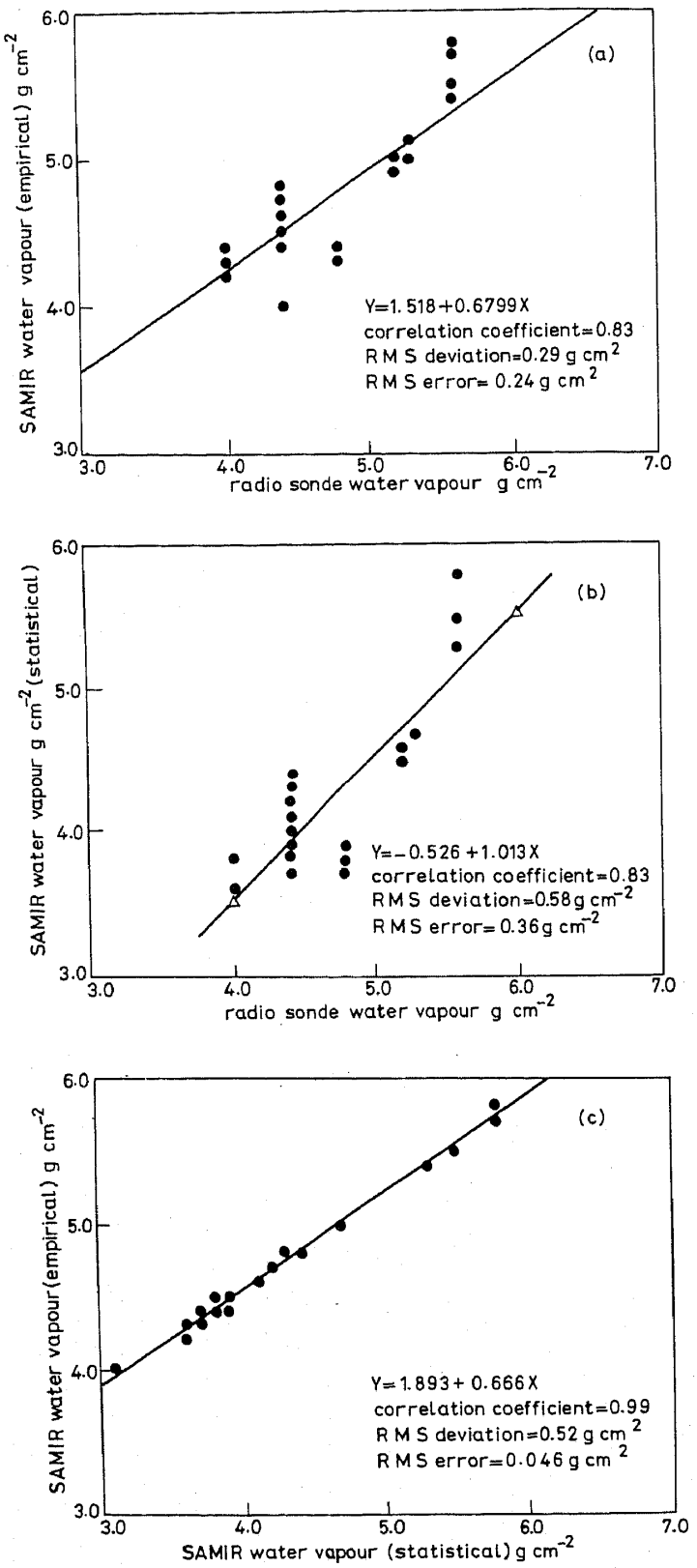


**Figure 12.** (**a**) Comparison of radiosonde derived water vapour (g/cm$^2$) versus SAMIR-water vapour (empirical) (g/cm$^2$). (**b**) Comparison of radiosonde derived water vapour (g/cm$^2$) versus SAMIR-water vapour (statistical). (**c**) Comparison of water vapour statistical *vs* empirical. (Gohil *et al* 1981a)

tropical cyclone were also observed and the maxima of wv was found in the cloud wall region, just outside the eye of the cyclone (Pandey *et al* 1982).

An attempt to improve wv and LW retrieval using few nonlinear terms in the linear regression approach was also made by Sharma *et al* (1981). Theoretical simulations showed an improvement in wv retrieval over that of linear method, but noisy brightness temperature measurements from SAMIR jeopardised the advantage over linear regression.

Gohil *et al* (1981) also attempted to estimate the rainfall rate over oceans using 19·35 GHz brightness temperature data. Scattering due to large hydrometers was not considered in the formulation, since at 19·35 GHz scattering effects are a small perturbation as shown by Wilheit *et al* (1977). In Gohil *et al*' s approach of estimating rainfall rate over oceans, cloud top height (known from IR measurements) was used as an additional predictor (figure 13). Clouds with different liquid water contents were also considered. Thus the approach developed for *Bhaskara* differed with earlier approaches and may provide improved rainfall rate estimation. However, the field of view, of SAMIR being large and the rainfall rate being a highly variable quantity in space and time, SAMIR is not optimally suited for rainfall rate estimation. Basic methodologies and approach could, however, be used for future generation of improved sensors. Rainfall rate being a complex and important problem, such types of study should be encouraged. Correlation between wind speed and 19·35 GHz brightness was also studied (Pandey *et al* 1980 and Sarkar *et al* 1981).

The applications of SAMIR data to land-based applications are not very encouraging. Some effort has been made to delineate flood region for the Luni River basin in Rajasthan, India (Pandey 1980). However, large scale terrain features could be analysed along with data obtained from other imaging sensors in visible and infrared region.

Basic radiative transfer formalism and methodologies developed for *Bhaskara-I* and SAMIR-I were used for analysing SAMIR-II data. In view of the discrepancies between theoretically calculated brightness temperature ($T_B$) and experimentally observed $T_B$, at SAMIR frequencies, attempts were made to improve the wind speed versus emissivity relationship (Sarkar 1983, Personal communication). A detailed comparison with other

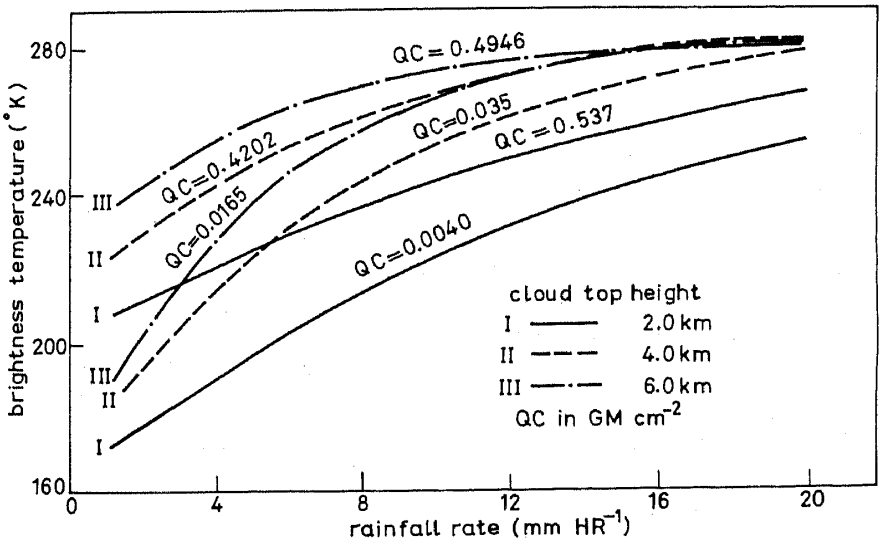


**Figure 13.** Oceanic rainfall rate versus 19 GHz brightness temperature for different cloud top heights and liquid water content (Gohil *et al* 1981).

emissivity models (Wilheit 1979; Pandey & Kakar 1982) is in progress. This was important, since the physics of electromagnetic interaction with other atmospheric constituents is well understood for general remote sensing applications. Calibration of raw radiometric counts to brightness temperature was also improved. It is anticipated that retrievals will improve with the incorporation of new emissivity versus wind relation in radiative transfer.

Three-channel retrievals (19, 22 and 31 GHz) and two-channel retrievals were also attempted. Figure 14 shows the SAMIR-II raw brightness temperature and retrieved water vapour for a typical pass of *Bhaskara-II*. Unlike, SAMIR-I, SAMIR-II data could not be thoroughly validated due to lack of planned *in situ* campaign. Although, SAMIR-II channels were not optimally chosen for wind speed retrieval, both theoretical as well as experimental efforts were made to understand the limitations of the frequencies for wind speed measurements (Sarkar & Bhandari 1983). More comparisons are being planned to arrive at the definite conclusions for wind speed retrieval.

The behaviour of 19·35 GHz $T_B$ data from SAMIR-II to the tropical cyclone has also been investigated by Bhandari (1983) using a differential approach. The effect of cyclone was brought out by subtracting the $T_B$ response for a quiet day. The method takes care of land/coastal contamination and gave satisfactory results of oceanic rainfall rate over the cyclonic region with broken clouds (Bhandari & Gohil 1983). Their method appears to be promising for studying tropical cyclones and latent heat release and require in-depth study and comparison with other satellite data. More theoretical and experimental work in this area is warranted.

Most of the analysis presented from *Bhaskara*–SAMIR data consider the data collected

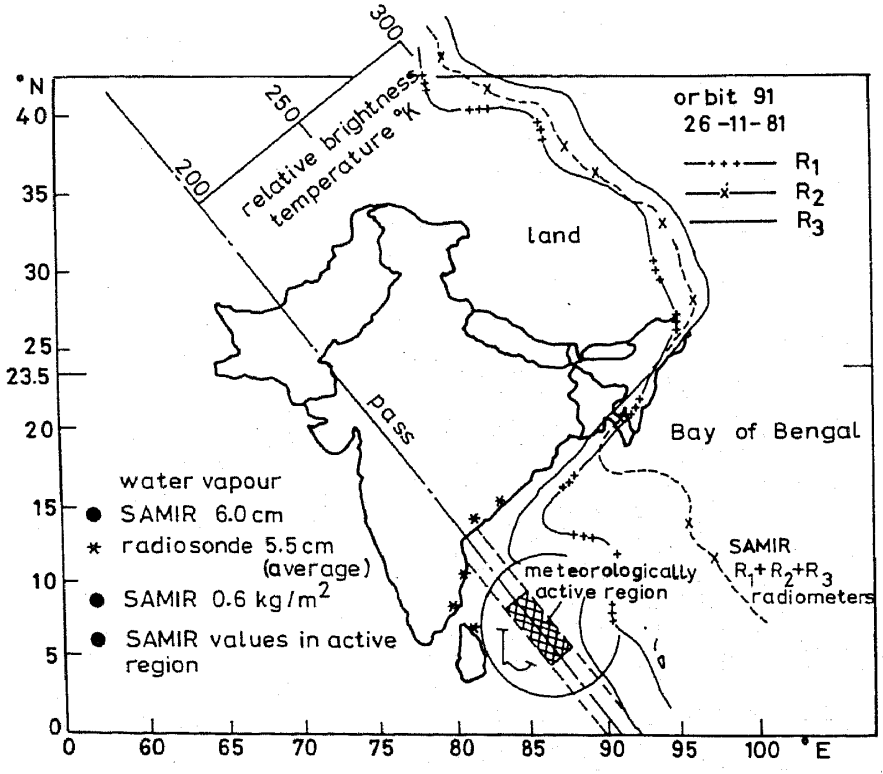


**Figure 14.** SAMIR-II observations on 26 November 1981 (orbit 91). SAMIR-II derived water vapour and nearby average radiosonde derived water vapour is also given.

near nadir direction. The data in alternate mode require decoupling of polarisations and compensation for sidelobes and are being attempted on the line suggested by Njoku (1980a) and used for SEASAT data analysis. Hariharan (1983) and Pathak *et al* (1983) have reviewed the work on SAMIR for its meteorological and oceanographic applications.

The authors thank B S Gohil, B M Rao, S M Bhandari, A Sarkar, D G K Murthy and M S Narayanan for their help in the preparation of this review article.

## References

Alishouse J C 1982 NOAA Tech. Report No. 90, National Oceanic and Atmospheric Administration, Washington DC

Allison L J, Rodgers E B, Wilheit T T & Fett R W 1974 *Bull. Am. Met. Soc.* **55** 1074

Atlas D & Thiele O 1982 Precipitation measurement from space, Workshop Rep., Goddard Space Flight Centre, Maryland, USA

Basharinov A E, Gurvich A S & Yegorov S T 1969 *Doklady Acad. Nauk. SSSR* **188** 18

Basharinov A E, Gurvich A S, Yegorov S T, Kurskaya A A, Matveyev D T & Shutko A M 1971 *Space Res. XI* (Berlin: Akademie-Verlag)

Bernstein R L (ed.) 1982 *J. Geophys. Res. Seasat Special Issue I. Geophysical Evaluation*, Vol. 87

Bhandari S M 1983 Private communication

Calla O P N, Raju G, Rana S S & Balasubramaniam S 1980 *J. IETE* **25** 321

Calla O P N, Raju G, Rana S S & Balasubramaniam S 1980 *J. IETE* **26** 243

Calla O P N, Raju G, Rana S S & Balasubramaniam S 1980 *J. IETE* **26** 332

Chahine M T 1977 *Inversion methods in atmospheric remote sounding* (ed.) A Deepak (New York: Academic Press) p. 67

Chandrasekhar S 1960 *Radiative transfer* (New York: Dover)

Desai P S 1982 MET-SN-14-82, Space Applications Centre, Ahmedabad.

Flower D A & Pekham G 1983 Private communication, Jet Propulsion Laboratory, USA

Gloerson P & Barath F T 1977 *IEEE J. Oceanic Engg.* **OE2** 172

Gohil B S, Hariharan T A, Pandey P C & Sharma A K 1981a *Int. J. Remote Sensing* **3** 235

Gohil B S, Sharma A K & Pandey P C 1981b Estimating rainfall rate over oceans using *Bhaskara*–SAMIR data, Presented at symposium on variations in the global water budget, Oxford, UK, August

Gohil B S, Sharma A K & Pandey P C 1981c *Proc. Indian Acad. Sci. (Earth & Planet Sci.)* **90** 263

Grody N C 1976 *IEEE Trans. Antennas Prop.* **AP24** 153

Grody N C, Hayden C M, Shieu W C C, Rosenkranz P W & Staelin D H 1979 *J. Geophys. Res.* **84** 3689

Hariharan T A 1983 *Proc. Indo-Soviet Symp. on Space Research*, ISRO, Bangalore, February

Haydu K J & Krishnamurthy T N 1981 *J. Appl. Meteor.* **20** 1177

Hofer R & Njoku E G 1981 *IEEE Trans. Geosci. Remote Sensing* **GE19** 178

Hofer R, Njoku E G & Waters J W 1981 *Science* **212** 1385

Hollinger J P 1971 *IEEE Trans. Geosci. Electron.* **GE-9** 165

Hollinger J P & Kenney J P 1976 NRL Memorandum 3308

Hollinger J P & Mannella R A 1973 *Science* **181** 54

Hughes Aircraft Co. 1979 *'Special sensor microwave/imagery (SSM/I) overall preliminary design review'* (Segundo, CA: Hughes Aircraft Co.)

Kunzi K F, Fisher A D, Staelin D H & Waters J W 1976 *J. Geophys. Res.* **81** 4965

Ledsham W H & Staelin D H 1978 *J. Appl. Meteor.* **17** 1023

Lenoir W B 1967 *J. Appl. Phys.* **38** 5283

Lipes R G 1980 JPL Publication 80–62 Jet Propulsion Laboratory, Pasadena CA 91109

Lipes R G, Bernstein R L, Cardove V J, Katsaros K G, Njoku E G, Riley A L, Ross D B, Swift C T & Wentz F J 1979 *Science* **204** 1415

Meeks M L & Lilley A E 1963 *J. Geophys. Res.* **68** 1683

Moore R K, Dellwig L F & Schmugge T 1975 *Radio Sci.* **10** 189

Moore R K & Young J D 1977 *IEEE J. Oceanic Engg.* **OE2** 309

Narayanan M S & Rao B M 1982 Unpublished

Njoku E G 1982 *Proc. IEEE* **70** 728
Njoku E G & Pandey P C 1982 Unpublished
Njoku E G, Christensen E J & Cofield R E 1980a *IEEE J. Oceanic Engg.* **OE-5** 125
Njoku E G, Stacey J M & Farath F T 1980b *IEEE J. Oceanic Engg.* **OE-5** 100
Pandey P C 1980 *Mausam* **31** 561
Pandey P C 1982 JPL Publication No. 82–95, Jet Propulsion Laboratory, Pasadena, California, USA
Pandey P C 1983 JPL publication No. 83–5, Jet Propulsion Laboratory, Pasadena, California, USA
Pandey P C, Gohil B S & Sharma A K 1980a *Proc. Indian Acad. Sci* (*Earth & Planet. Sci.*) **89** 293
Pandey P C, Gohil B S & Sharma A K 1980b *Proc. Indian Acad. Sci* (Earth & Planet. Sci.) **89** 231
Pandey P C, Gohil B S & Sharma A K 1980c *Mahasagar Bull. National Inst. Oceanogr.* **13** 91
Pandey P C, Gohil B S & Sharma A K 1981 *Mausam* **32** 17
Pandey P C, Sharma A K & Gohil B S 1981 *Proc. Indian Acad. Sci.* (*Earth & Planet. Sci.*) **90** 105
Pandey P C & Kakar R K 1982 *IEEE J. Oceanic Engg.* **OE7** 135
Pandey P C & Kakar R K 1983 *IEEE Geoscience Remote Sensing* **GE-21** 208
Pandey P C & Kniffen S 1982 JPL Publication No. 82–89 Jet Propulsion Laboratory, Pasadena, California, USA
Pathak P N, Desai P S & Hariharan T A 1983 *Indian J. Radio Phys.* (in press)
Prabhakara C, Chang H D & Chang A T C 1982 *J. Appl. Meteor.* **21** 59
Rosenkranz P W 1978 *Radio Sci.* **13** 1003
Rosenkranz P W & Staelin D H 1982 *J. Appl. Met.* **21** 1364
Rosenkranz P W, Barath F T, Blinn J C, Johnston E J, Lenovi W B, Stalin D H & Waters J W 1972 *J. Geophys. Res.* **77** 5833
Ruprecht E & Gray W M 1976 *Tellus* **28** 414
Sarkar A 1983 Private communication
Sarkar A & Bhandari S M 1983 Unpublished
Savage R C 1976 *The transfer of thermal microwaves through hydrometers* Ph.D. Thesis, University of Wisconsin, Madison, USA p. 147
Schmugge T J 1978 *J. Appl. Meteor.* **17** 1549
Schmugge T J, Gloersen P, Wilheit T & Geiger F 1974 *J. Geophys. Res.* **79** 317
Sharma A K, Gohil B S & Pandey P C 1981 Estimation of atmospheric water vapour content with *Bhaskara* microwave radiometer data using nonlinear regression formulations, Presented at the Symposium on variations in the global water budget, Oxford, August
Sheaerer G & Wilheit T T 1979 *Radio Sci.* **14** 371
Staelin D H 1981 *IEEE Trans. Antennas Propagat.* **AP-29** 683
Staelin D H, Cassel A L, Kunzi K F, Pettyjohn R L, Poon R K L & Rosenkranz P W 1976 *J. Atmos. Sci.* **32** 1970
Staelin D H, Kunzi K F, Pettyjohn R L, Poon R K L & Wilcox R W 1975 *J. Appl. Meteor.* **15** 1204
Swanson P N & Riley A L 1980 *IEEE J. Oceanic Engg.* **OE-5** 116
Tomiyasu K 1974 *Proc. IEEE* **62** 1
Tsang L & Kong J A 1976 *Radio Sci.* **11** 599
Ulaby F T 1976 *IEEE Trans.* **AP-24** 112
Ulaby F T, Dellwig L F & Schmugge T 1975 *Radio Sci.* **10** 11
Ulaby F T, Moore R K & Fung A K 1981 *Microwave remote sensing: Fundamentals and radiometry* (Massachusetts: Addison Wesley) Vol. 1
Waters J W 1976 *Methods in experimental physics* (ed.) M L Meeks (New York: Academic Press) Vol. 12, p. 172
Waters J W, Kunzi K F, Pettyjohn R L, Poon R K L & Staelin D H 1975 *J. Atmos. Sci.* **32** 1953
Waters J W, Wilson W J & Shimabukuro 1976 *Science* **191** 1174
Waters J W & Wofsy S C 1978 in *High resolution passive microwave satellites*, (eds) D H Staelin & P W Rosenkranz (Cambridge: MIT Res. Lab. Electronics)
Weinman J A & Davies R 1978 *J. Geophys. Res.* **83**
Wentz F J 1983 *J. Geophys. Res.* **88** 1892
Wentz F J, Christensen E J & Richardson K A 1981 *Oceanography from space* (New York: Plenum Press) p. 741
Wilheit T T 1979 *IEEE Trans. Geosci. Remote Sensing* **GE17** 244
Wilheit T T & Chang A T C 1980 *Radio Sci.* **15** 525
Wilheit T T, Chang A T C, Rao M S V, Rodgers E B & Theon J S 1977 *J. Appl. Meteor.* **16** 551